Sensors and Actuators B 174 (2012) 332–341

Contents lists available at SciVerse ScienceDirect

Sensors and Actuators B: Chemical

journal homepage: www.elsevier.com/locate/snb

Fabrication of biomimetic device with PS-*b*-PNIPAAm copolymer pillars mimicking a gecko foot pad

Jem-Kun Chen[a,*], Jing-Hong Wang[a], Chih-Chia Cheng[b], Fu-Hsiang Ko[b]

[a] Department of Materials Science and Engineering, National Taiwan University of Science and Technology, 43, Sec. 4, Keelung Rd, Taipei 106, Taiwan, ROC
[b] Department of Materials Science and Engineering, Department of Applied Chemistry, National Chiao-Tung University, Hsinchu 300, Taiwan

ARTICLE INFO

Article history:
Received 29 May 2012
Received in revised form 2 August 2012
Accepted 21 August 2012
Available online 28 August 2012

Keywords:
PS-*b*-PNIPAAm brush
Biomimetic surfaces
Thermally switchable adhesion
Multi-layer thin film

ABSTRACT

Inspired by the climbing aptitude of geckos, a gecko's foot pad can alternately attach to and detach from almost any kind of surface. We firstly fabricated a multi-layer thin film with electrodes as a thermal device that could adjust the surface temperature by applying voltage. We sequentially used very-large-scale integration (VLSI) process and atom-transfer radical-polymerization (ATRP) process to generate well-defined pillar patterns of polymerized styrene as seta analogues and successively grafted n-isopropylacrylamide (NIPAAm) as thermally responsive terminating of the pillars to mimic the configuration of a real gecko's foot pad. Our fabrication strategy exploits surface textures of polystyrene (PS) and thermally responsive terminating of PNIPAAm, which could generate alternately ca. 88.1 and 11.3 nN of adhesive force at 0.2 and 2 V of applying voltage, respectively. The results indicate that the adjustable adhesive ability of the copolymer brushes could approach the climbing aptitude of a gecko much more closely through voltage tuning. The advantage of the processing strategy described here is the potential to fabricate a device of an artificial foot pad to mimic the climbing aptitude of geckos vividly.

1. Introduction

The amazing aptitude of some insects and lizards to stick readily and rapidly to almost any surface (whether hydrophilic or hydrophobic, rough or smooth, dry or wet) has attracted widespread research interest with respect to the development and application of biomimetic structures. Bioadhesion has received much experimental and theoretical attention recently [1] – especially that of geckos [2], the largest animals capable of running on walls and ceilings [3]. The attachment pads of many insects and geckos are covered with long micro- to nanosized hairs with characteristic geometries and mechanical properties. This remarkable surface topography enables these animals to firmly attach to and readily detach from almost any kind of surface. The adhesive strategy of the gecko relies on foot pads composed of specialized keratinous foot-hairs called setae, which are subdivided into terminal spatulae of approximately 200 nm [4,5]. Contact between the gecko foot and an opposing surface generates adhesive forces that are sufficient to allow the gecko to cling onto vertical and even inverted surfaces. Although strong, the adhesion is temporary, permitting rapid detachment and reattachment of the gecko foot during locomotion.

The adhesive forces of the gecko have been observed to be on the order of 40 μN or more per seta [6] and 10 nN per spatula [7]. Gecko adhesion has been explained as arising from weak secondary bond forces such as van der Waals. However, adhesion of a single spatula varies as a function of humidity and is dramatically reduced under water [8], suggesting some contribution from capillary forces. Contact mechanics arguments have been invoked to explain the subdivision of the seta contact surface into multiple independent nanosized spatulas, giving rise to enhancement of the mechanical behavior. Inspired by the above biological systems, various kinds of patterned surfaces with large numbers of regular micro- to nanoscale structures, including cylindrical or conical pillars (columns or posts) with flat, spherical, toroidal, or concave ends, have been designed and fabricated aimed at enhancing adhesion properties [9]. Indeed, a strong effect of contact shape was identified which can overshadow the influence of contact size. Most of these literatures reported approaches to merely pursue extremely high bioattachment or superhydrophobicity and superhydrophilicity of a nanostructured surface [10]. Without adjustable adhesive ability, these nanostructured surfaces may stick to a surface firmly, but they could not detach from a surface easily.

Researchers have attempted to capture these properties of gecko adhesive in synthetic mimics with nanoscale surface features reminiscent of setae [11,12]; however, maintenance of adhesive performance over many cycles has been elusive [13,14], and gecko adhesion is greatly diminished upon full immersion in water [8]. Synthetic gecko adhesives that exhibit dry adhesion have been

* Corresponding author. Tel.: +886 2 27376523; fax: +886 2 27376544.
E-mail address: jkchen@mail.ntust.edu.tw (J.-K. Chen).

0925-4005/$ – see front matter © 2012 Elsevier B.V. All rights reserved.
http://dx.doi.org/10.1016/j.snb.2012.08.044

fabricated from polymers [11] as well as multiwalled carbon nanotubes [15]. However, maintenance of adhesion during repetitive contacts has only been demonstrated for a few contact cycles [8,14]. The use of polymers as building blocks for surface modification allows the preparation of "smart" or responsive surfaces that function based on conformational changes in the polymer backbones [16,17]. Stimuli-responsive hydrogels, which undergo large reversible volume changes in response to variations in environmental factors, are excellent candidates for various optical or biological detection applications [18–22]. To mimic a gecko foot pad vividly, the adjustable adhesive ability of simultaneously attaching to and detaching from a surface through internal stimuli is necessary, but not merely high adhesion or an excellent lotus effect. In this context, we focused on the fabrication of an artificial foot pad device with copolymer pillars and then the testing of its stimuli-responsive adhesion through switching voltages [23]. The pillar arrays of block copolymer brushes were prepared from poly(*N*-isopropylacrylamide) (PNIPAAm) on patterned polystyrene (PS) pillar arrays to mimic setae with tips containing spatulas [1]. The wettability of PNIPAAm-grafted surfaces exhibits a temperature-dependent transition near the lower critical solution temperature (LCST) of PNIPAAm (ca. 32 °C) [24]. Below the LCST, the PNIPAAm chains are strongly hydrated and possess an extended conformation; when heated above the LCST, however, the polymer undergoes a phase transition to a collapsed morphology, due to dehydration. Our goal for this paper is to fabricate a biomimetic device for thermally responsive adhesion in biological systems and to guide the design of bio-inspired artificial analogues.

2. Experimental

2.1. Materials

Single-crystal silicon wafers, Si(100), polished on one side (diameter: 6 in.) were supplied by Hitachi, Inc. (Japan) and cut into 0.6 in. × 0.6 in. samples. The Si substrates were oxidized to generate the hydroxyl groups by a cleaning process in pervious report [25]. Styrene (Acros Organics Co.) was washed three times with a 5 wt % sodium hydroxide solution and twice with distilled water. After drying with anhydrous magnesium sulfate, the monomer was purified by distillation under reduced pressure and stored in a refrigerator immediately after distillation. *N*-isopropyl acrylamide (NIPAAm, Acros Organics Co.) was recrystallized from a toluene/hexane solution (50%, v/v) and dried under vacuum prior to use. Other materials used for graft polymerization, 3-aminopropyltriethoxysilane (AS) and 2-bromo-2-methylpropionyl bromide (BB), copper(I) bromide, copper(II) bromide, triethylamine (TA), and 1,1,4,7,7-pentamethyldiethylenetriamin (PMDETA), were purchased from Acros Organics Co. PMDETA, AS, and BB were purified through vacuum distillation prior to use. All other chemicals and solvents were of reagent grade and purchased from Aldrich Chemical Co.

2.2. Fabrication of the biomimic device with copolymer pillars

Fig. 1 outlines our basic strategy for the fabrication of the biomimetic device with PS-*b*-PNIPAAm copolymer pillars, using a very-large-scale integration (VLSI) process developed in a previous study [26]. A: After soft-etching at 200 W in Ar plasma, the aluminum thin film was deposited through radio frequency (RF) reactive sputtering (ULVAC Sputter SBH-3308RDE) with Ar under 1500 W of RF power for 20 min. The base pressure in the chamber of physical vapor deposition was 4.6×10^{-7} torr and the target-to-substrate distance 150 mm. The thickness of the aluminum layer on the silicon surface was ca. 810 nm. B: A silicon nitride thin film was deposited by plasma-enhanced chemical vapor deposition (PECVD, 100 PECVD cassette system) under the mixture gases of SiH_4 and N_2 on the aluminum thin film surface to be a buffer layer. Silicon oxide thin film was sequentially deposited on the nitride layer by PECVD under tetraethyl orthosilicate (TEOS) for reacting with the initiator of atom transfer radical polymerization (ATRP). The thicknesses of the nitride and silicon oxide were about 350 and 220 nm, respectively. We applied a voltage on the aluminum thin film for controlling the hydrophilic and hydrophobic properties of the tethered PNIPAAm by tuning the temperature of the substrate [23]. C: The Si wafer was treated with hexamethyldisilazane (HMDS) in a thermal evaporator (Track MK-8) at 90 °C for 30 s to transform the hydroxyl groups on the surface of the substrate into an inert film of $Si(CH_3)_3$ groups (Scheme 1). The photoresist was spun on the HMDS-treated Si wafer at a thickness of ca. 350 nm. 1 μm-resolution contact hole array on the photoresist were successively patterned by lithography process. D: The sample was then subjected to OPT to form hydroxyl groups from the HMDS-treated surface. OPT caused the bottom surface to become chemically modified (strongly hydrophilic or polar) only in the areas not covered by the photoresist [27]. E: To immobilize the ATRP initiator, the Si substrate was immersed in a 0.5% (w/v) solution of AS in toluene for 2 h at 50 °C. The AS units assembled selectively onto the bare regions of the bottom Si–OH surface after OPT, where it reacted with Si—O and Si—O—O species. The sample was immersed in both of 2% (v/v) solution of BB and TA in toluene for 8 h at 20 °C. After reaction, the wafers were placed in a Soxhlet apparatus to remove any nongrafted material. This procedure resulted in a surface patterned with regions of AS–BB for ATRP and regions of photoresist. ATRP of monomer mixture including 80 mol% styrene and 20 mol% 1,4-divinylbenzene (DVB) was carried out according to a previously reported method [1]. DVB, which contains two reactive vinyl groups, is an excellent cross-linker for the preparation of 3-D polymer networks. For the preparation of cross-linked PS brushes on the Si–AS–BB surface, the mixture monomer, Cu(I)Br, $CuBr_2$, and PMDETA were added to toluene. The solution was stirred and degassed with argon for 15 min at 90 °C. The solution was successively transferred to a flask containing Si—AS—BB silicon wafers, and extra BB was added by syringe. Polymerization of the monomer mixture was allowed to proceed at 70 °C for 24 h inside the square hole array of photoresist to generate pillars as the basic structure of biomimetic surfaces. Afterward, the wafers were taken out of the polymerization solution and rinsed thoroughly with toluene. To remove physically adsorbed polymer, the wafers were Soxhlet extracted with dichloromethane for 24 h, cleaned ultrasonically in dichloromethane, and finally dried under a flow of nitrogen. F: The Si–PS surfaces were used as macroinitiators for the subsequent surface-initiated ATRP of PNIPAAm to produce diblock copolymer brushes. Surface initiated ATRP grafting of NIPAAm was carried out in a glass vessel purged with nitrogen. NIPAAm, PMDETA, and Cu(I)Br, $CuBr_2$ were dissolved in dimethylformamide (DMF). The reaction solution was sonicated for 2 min and then was added to the glass vessel in which the macroinitiator functionalized wafers were placed. Polymerization was carried out at room temperature under nitrogen purging for 12 h inside the square hole array of photoresist for attachment of the thermally responsive property on the contact regime of pillars. After the desired period of time, the obtained PS-*b*-PNIPAAm grafted substrate possessing multi-layer thin film was removed from the solution, rinsed with abundant deionized water to remove unreacted monomer and PNIPAAm that was not grafted, and then dried under a flow of nitrogen. G: Finally, the remaining photoresist was removed from the PS-*b*-PNIPAAm-grafted silicon surface by rinsing with slight basic aqueous solution, leaving behind the chemically nanopatterned PNIPAAm-*b*-PS brush surface.

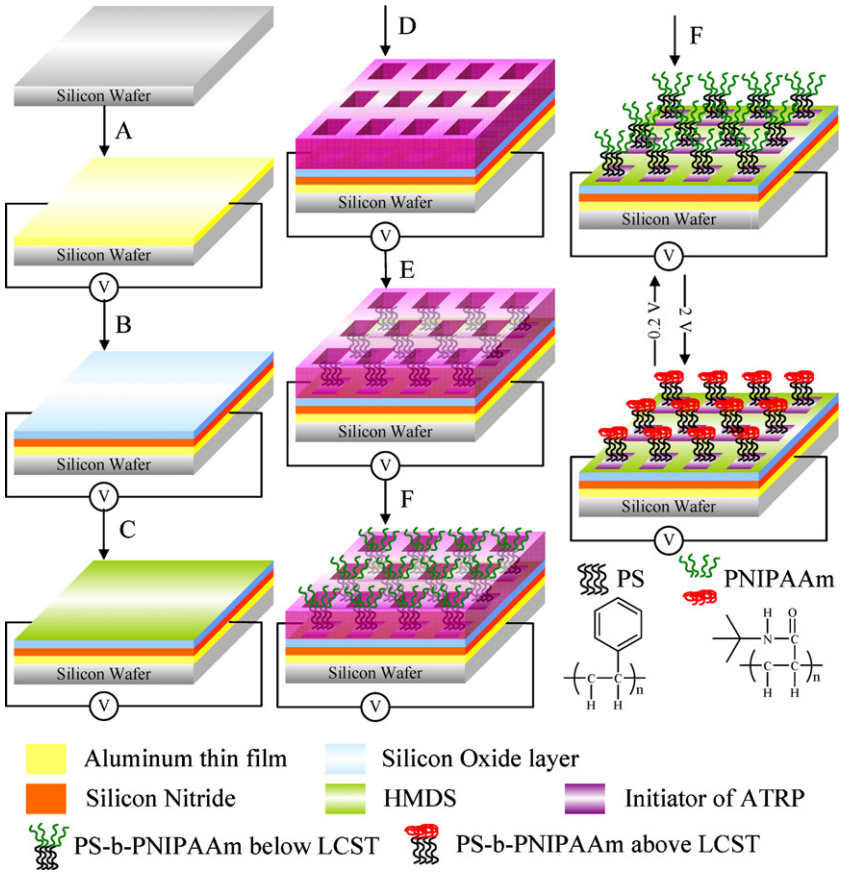

Fig. 1. Schematic representation of the process used to fabricate a multi-layer thin film surface chemically micropatterned with PS-*b*-PNIPAAm brushes. (A) An aluminum thin film was deposited through radio frequency reactive sputtering by using Ar as the gases for 20 min. A voltage was applied on the aluminum thin film for temperature tuning. Sequentially, a nitride thin film was deposited by plasma-enhanced chemical vapor deposition on the aluminum thin film surface to be a buffer layer. (B) Silicon oxide thin film was then deposited on the nitride layer using tetraethyl orthosilicate (TEOS) for reacting with the initiator of ATRP. (C) Si wafer treated with HMDS in a thermal evaporator. (D) Photoresist spin-coated onto the Si surface presenting $Si(CH_3)_3$ groups. Electron-beam lithography used to pattern the photoresist as hole arrays possessing various aspect and duty ratios on the surface. OPT used to chemically modify the exposed regions presenting $Si(OCH_3)_3$ groups and to convert the topographic photoresist pattern into a chemically modified surface pattern. The silicon oxide layer was treated sequentially with AS and BB, to transform the hydroxyl groups into an initiator film of ATRP. The initiator of ATRP selectively assembled onto bare regions of the thin film surface. Sample grafting, through surface-initiated ATRP of a mixture of styrene and DVB, from the functionalized areas of the patterned initiator to form pillar arrays of cross-linked PS brushes. (E) Object grafting, through surface-initiated ATRP of NIPAAm from the macroinitiator on the top of the pillars, to generate PS-*b*-PNIPAAm copolymer brush pillars. (F) Photoresist removed through treatment with a slightly basic aqueous solution. The pillar arrays of the copolymer brushes on the surface exhibited thermally dependent adhesive properties between 0.2 and 2 V.

2.3. Characterization of the PS-b-PNIPAAm copolymer pillars on the multi-layer thin film

The chemical composition of the modified silicon surfaces was determined with a photoelectron spectrometer (XPS) (XPS; Scientific Theta Probe, UK). The thicknesses of the copolymer-modified multi-layer thin films were analyzed using ellipsometry (SOPRA SE-5, France). In addition, the tethered PS-*b*-PNIPAAm copolymer was stripped from the surface through immersion in HF solution (5 wt%) for 5 min at room temperature. The stripped PS-*b*-PNIPAAm copolymer was analyzed using gel permeation chromatography (GPC) after purification through extensive dialysis against DI water, performed using a VISCOTEK-DM400 instrument equipped with a LR 40 refractive index detector. Monodisperse polymer standards (Polymer Lab, Agilent) were used to generate a calibration curve. The monomer conversion was determined gravimetrically. The morphology of the tethered PNIPAAm brushes was measured using atomic force microscopy (AFM; Veeco Dimension 5000 scanning probe microscope) and high-resolution scanning electron microscopy (HR-SEM, JEOL JSM-6500F, Japan).

To investigate the surface morphologies of tethered PS-*b*-PNIPAAm pillars, the samples were immersed in deionized water for 3 h and then lyophilized prior to AFM examination. Friction and adhesive force were measured experimentally by an AFM/FFM, using the contact mode. Commercially available rotated monolithic silicon probe, symmetric tip shape with a nominal spring constant of 3 N/m, and a coated tip with a curvature radius of less than 10 nm was employed. Friction forces were obtained from friction-load line on each surface with a scan frequency of 1 Hz and a scan size of 80 μm × 80 μm. The output voltages were directly used as frictional forces. No attempt was made to calibrate the torsion force constant. Repeated measurements were within 1% of the average value for each sample. Adhesive force which is also called pull-off force was obtained from the force–distance curve and was calculated by $F = KcZp$ [28], where Kc is the force constant of cantilever and Zp is the vertical displacement of the piezotube. For all measurements, the same tip was used in this study. All the measurements were performed at room temperature with a relatively humidity of 35%. Repeated measurements were within 5% of the average value for each sample.

The static water contact angles (SWCAs) of the functionalized silicon surfaces were measured using the sessile drop method on an optical SWCA meter. The SWCA was determined by fitting a Young–Laplace curve around the drop. The experiment was performed under normal laboratory ambient conditions, 25 °C, and 30% relative humidity. The mean value was calculated from at least 10

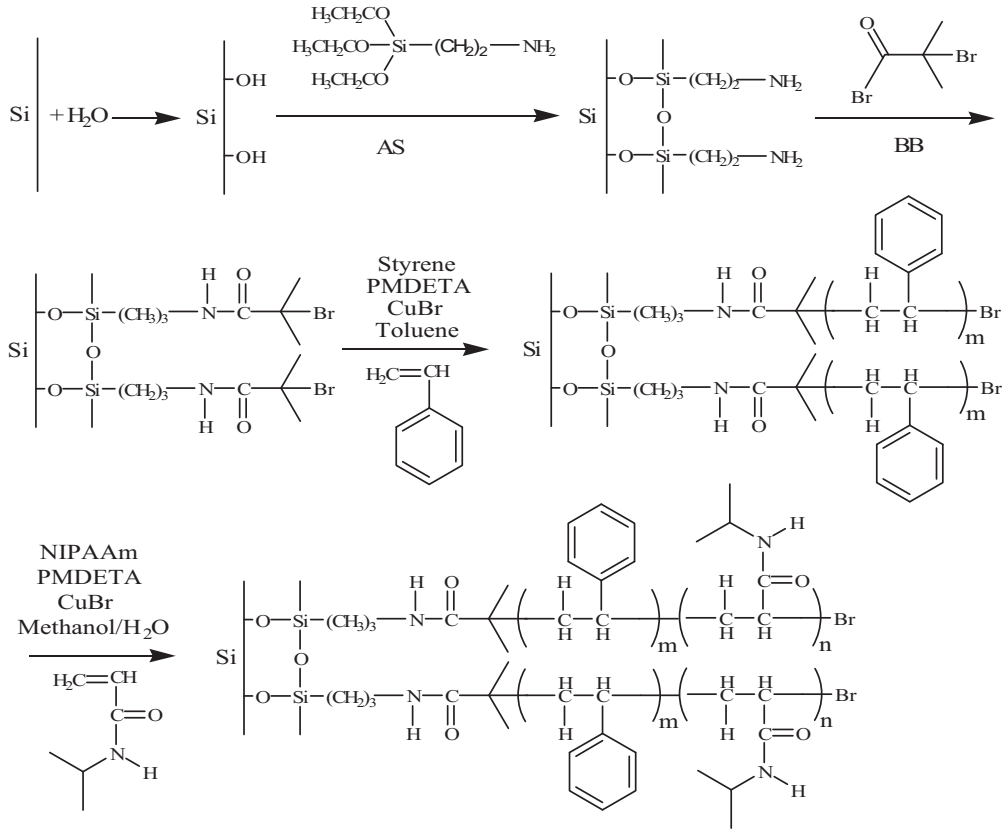

Scheme 1. Synthetic route toward Si wafers presenting PS-*b*-PNIPAAm brush prepared through ATRP.

individual measurements and the measurement error was less than 3°. In addition, it is well known that a heterogeneous surface (chemically or geometrically) usually shows contact angle hysteresis [29]. That is, for a geometrically rough surface, contact angle hysteresis originates primarily from the rough contact interface that depends upon the contact area of water with the structured surface. The earliest works to model liquid drop on a roughness surface can be contributed to Wenzel [30] and Cassie and Baxter [31]. In this case, liquid fills up the rough surface to form a completely wetted contact with the surface and this phenomenon is known as the Wenzel state. On the other hand, a liquid droplet sits on a composite surface composed of solid and air which is also known as the Cassie state. It is well understood that there is no unique contact angle to characterize any given surface. The observed equilibrium contact angles always fall between the advancing and receding contact angles. The contact angle hysteresis $\Delta\theta$, defined as the difference between advancing and receding contact angles ($\Delta\theta = \theta adv - \theta rec$), can be used to conclude the state of a liquid droplet. If the contact angle hysteresis is small, then the droplet would be at the Cassie state. On the other hand, if the contact angle hysteresis is large, then the droplet would be at the Wenzel state. This implies that the contact angle hysteresis is responsible for the pinning of liquid droplets on a surface.

3. Results and discussion

3.1. Fabrication of the thermal device of the multi-layer thin film

The surface temperatures of the multi-layer thin film under various applying voltages are shown in Fig. 2a. The surface temperature increases linearly with the applying voltage suggesting a stable and a predictable system. Generally speaking, applying voltage on multi-layer thin film for temperature adjusting will neither

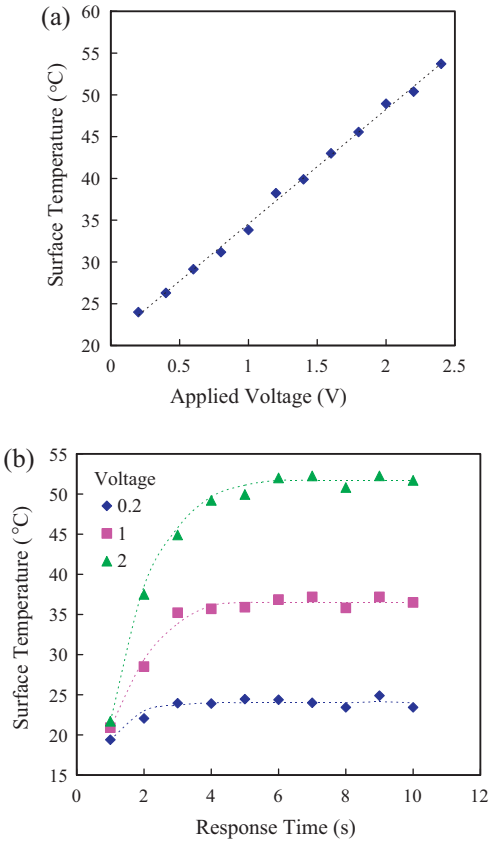

Fig. 2. Dependence of surface temperature of the multi-layer thin film surfaces with (a) applying voltages and (b) response times, respectively.

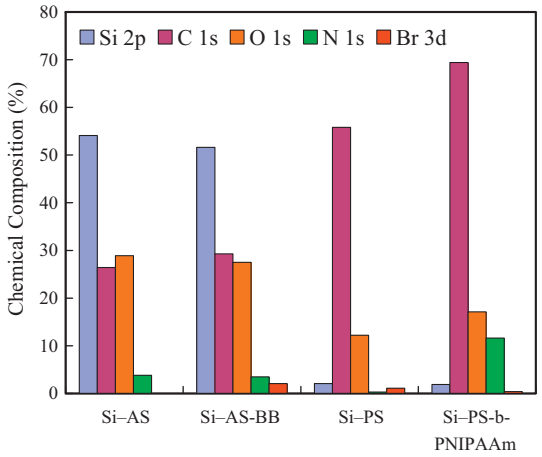

Fig. 3. Chemical composition of the Si–AS, Si–AS-BB, Si–PS, and Si–PS-*b*-PNIPAAm surfaces, determined from XPS core level spectral area ratio.

use strong voltage nor use long response time. This chart provides a reasonable and valuable reference for evaluation of surface temperature under various applying voltages on the device. Basically, the temperature is proportional to a continuously applied voltage and accumulated time. However, the voltage applying on the device could adjust automatically by a pulse mode to maintain the target temperature on device. Therefore, the target temperature could achieve by specific voltage efficiently. The surface temperature was stable after several minutes or hours. The surface temperature can be adjusted from 24 to 54 °C, obtained by measuring five points on the surface, by increasing applying voltages. The low applying voltage is generally used for steady state of temperature without any current impulse inside the solid state substrate. Therefore, the 0.2 and 2.0 V were chosen to adjust the surface temperature between 24 and 48 °C, showed very promising temperatures below and above LCST of PNIPAAm, respectively. As shown in Fig. 2b, its response time was fast and before 5 s it achieved a stable surface temperature. The high efficiency process condition might be good for applications especially for thermal devices. Since we already achieved the target temperatures, we did not try to reduce parameter of the multi-layer thin film or gas selection in order to reduce the response time.

3.2. Formation of the PS-b-PNIPAAm copolymer-modified multi-layer thin film surface

To prepare polymer brushes on the thin film surface it is necessary for us to immobilize a uniform and dense layer of initiators on the Si surface [32,33]. Fig. 3 displays chemical composition of the Si–AS, Si–AS–BB, Si–PS, and Si–PS-*b*-PNIPAAm surface, determined from XPS core level spectral area ratio. XPS analysis confirmed the changes in the chemical composition of the Si surface after grafting. For the PS-grafted surface, we observed only C atoms, suggesting that the surface was completely covered with a layer of PS [34]. Because the thickness of the grafted PS layer was much greater than the sampling depth (ca. 10 nm) of the XPS system, the N1s and O1s components of the initiator were not discernible after the addition of the PS block. Because PNIPAAm comprises C, H, O, and N atoms, we observed the signals of its N1s and O1s components after grafting, appeared apparently in Fig. 3.

We established the surface polymerization kinetics on the surface under two assumptions: (i) the grafting rate was sensitive to the concentration of the monomer and (ii) the grafting species deactivated completely over a period of several hours. As a result, the grafting polymerization kinetics on the surface was defined using Eqs. (1) and (2) [34]

$$d = \frac{Nm_0}{\rho} = \frac{k_p M_0 I_0 m_0}{k_d \rho}(1 - e^{-k_d t}) \quad (1)$$

$$M_s = \frac{Nm_0 A}{I_0 A} = \frac{k_p M_0}{k_d}(1 - e^{-k_d t}) \quad (2)$$

where d is the ellipsometric thickness of the film; ρ is the density of the polymer; m_0 is the mass of the monomer unit; I_0 is the initial number of active grafting sites per unit area; k_p is a propagation rate in a second-order reaction; k_d is the rate of deactivation (irreversible) in a first-order reaction; N is the total number of polymerized monomer units on the surface per unit area; M is the concentration of the monomer in solution; and M_s is the surface-average molecular weight. In Eq. (1), the ellipsometric thickness (d) increases linearly with the concentration of the monomer in solution (M). Fig. 4a displays the thicknesses of the PS-*b*-PNIPAAm brush grafted for various times onto the Si–AS–BB surfaces. Our PS-grafted layer had a thickness of 225 nm, which is greater than the value reported elsewhere [25], presumably because we performed the Si–ATRP of styrene within the square hole array of the photoresist. The results ascribe that the Si–ATRP of styrene was carried out inside the square hole array of photoresist. In general, the grafting species on surface-tethered polymer brush chain with lower degree of freedom deactivated due to the entanglement of polymer chains [18]. The halogen groups of chain end consecutively stocked on the upper part of the polymer brushes due to the besieging of the photoresist, enhancing the reactivity of halogen groups. We obtained additional evidence for the controlled polymerization from stripped PS formed from the surface initiator. The ATRP of NIPAAm was then carried out in DMF with the grafted PS brushes as the macroinitiator. Free BB initiator was added to the polymerization medium to generate a sufficient concentration of the deactivator copper(II) species; this is necessary for the formation of homogeneous films with grafts of controlled length, especially in the beginning stages of the ATRP process [35]. Because of length of the copolymer brush over the thickness of the photoresist, the thicknesses of the copolymer brush grafting over 36 h reached an approximately constant value. In addition, the increase in thickness of approximately 100 nm, relative to the initial PS layer, resulted from the formation of PNIPAAm blocks. Fig. 4b displays the linear relationship between $\ln([M_0]/[M])$ and time for PS and PNIPAAm, respectively, where $[M_0]$ is the initial monomer concentration and $[M]$ is the monomer concentration for styrene and NIPAAm. The concentration of the growing species remained constant, and first-order kinetics were obtained. The data shown in Fig. 4a can be fit well by Eq. (1) for PS and PNIPAAm before and after 24 h, respectively. The values derived from the fit are $(k_p M/k_d)(m_0 I_0/\rho) = 332$ and 90 nm for PS and PNIPAAm, respectively, obtained by grafting for 48 h as infinite time, and $k_d = 1.4 \times 10^{-5}$ and 3.3×10^{-5} s^{-1} for PS and PNIPAAm, respectively. The number of polymer chains bound per square centimeter should be approximately equal to the number of alkylsiloxane initiators per unit area. For linear alkylsiloxanes with 10–18 carbons, the area per R-Si is ~2.1 nm^2 at full coverage [36]. We used 104.2 g/mol and 1.052×10^{-21} g/nm^3 as m_0 and ρ (an approximate value for the density of the polymer) for bulk PS, 113 g/mol and 0.788×10^{-21} g/nm^3 for bulk PNIPAAm. The estimate of k_p obtained from these values lies in the range of $\sim 1.3 \times 10^{-2}$ and $\sim 5.3 \times 10^{-3}$ s^{-1} M^{-1} for PS and PNIPAAm, respectively. A rough estimate for the unitless terms $k_p M/k_d$ (the effective chain length for $M = 1.5$ mol/L) are calculated to be ~1423 and ~239 for PS and PNIPAAm, respectively, on the basis of the above assumptions. Furthermore, we obtained surface-average molecular weights (M_s) of PS brush on the silicon surface from Eq. (2) with 24 h and additional data of number-average molecular weight for the stripped

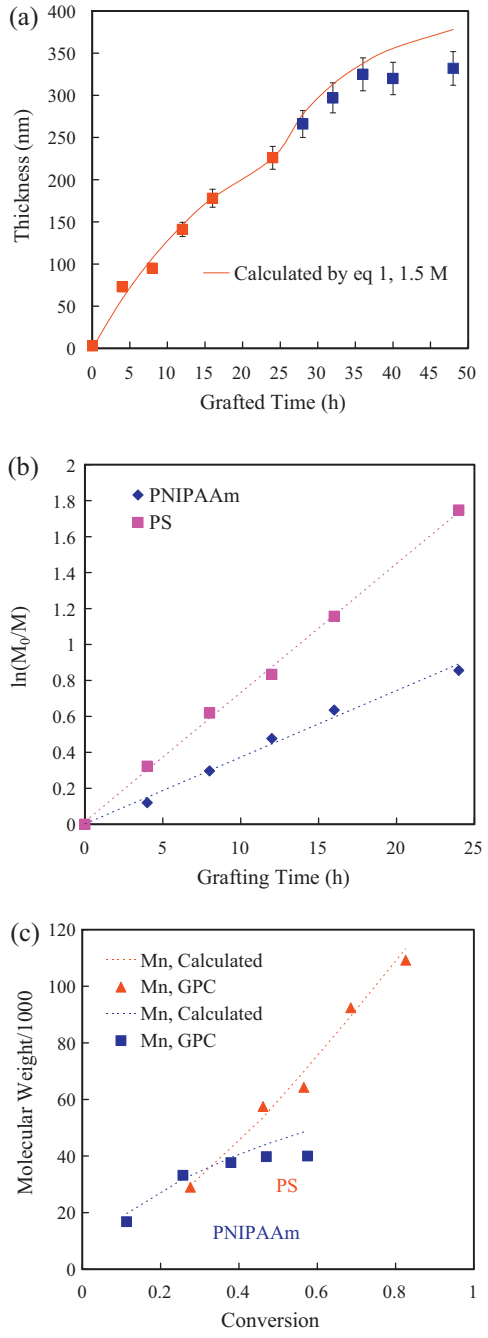

Fig. 4. (a) Ellipsometric thickness of the copolymer layer, grown from the Si–AS–BB surface via ATRP, recorded as a function of grafting time in the monomer solution for monomer concentration of 1.5 M. The plots were fitted to surface grafting polymerization kinetic thickness [$d = (k_{p,PS}M_{PS}I_0m_{0,PS}/k_{d,PS}\rho_{PS})(1-e^{-k_{d,PS}t}) + (k_{p,PNIPAAm}M_{PNIPAAm}I_0m_{0,PNIPAAm}/k_{d,PNIPAAm}\rho_{PNIPAAm})(1-e^{-k_{d,PNIPAAm}t})$]. Relationships between (b) $\ln([M_0]/[M])$ and the grafting times and (c) number-average molecular weight (M_n) of stripped copolymer by GPC recorded as a function of monomer conversion for PS and PNIPAAm. The plots were fitted to surface grafting polymerization kinetic M_s [$M_s = k_pM/k_d(1-e^{-k_dt})$].

PS brushes as shown in Fig. 4c. The M_n from stripped PS and PNIPAAm can be fit well by Eq. (2) for monomer concentrations of 1.5 M. The polydispersity index (PDI, M_w/M_n) of the stripped PS and PNIPAAm were ca. 1.04 and 1.21, respectively, obtained from GPC measurement. Because of the deactivation of the grafting species, the thicknesses of the copolymer brushes after 36 h of polymerization reached an approximately constant value corresponded to the thickness. The grafting density in chains per surface area (D_s, chains/nm^2) may be calculated according to the equation:

$$D_s = d\rho N_a/M_n$$

where N_a is Avogadro's number (molecules/mol). We obtained grafting density of 0.139 chains/nm^2 from the PS brushes grafted for 24 h. The grafting density increase to 0.284 chains/nm^2 after sequential grafting PNIPAAm for 12 h. SWCA measurements revealed the wettabilities of the functionalized thin film surfaces at the various stages, consistent with those from previous studies [28]. After modification with PNIPAAm, the surface exhibited thermoresponsive properties, with SWCAs of 41.6 and 82.7° at 0.2 and 2.0 V, respectively. This strong temperature dependence of the surface wettability further confirmed the presence of the PNIPAAm layer of the copolymer.

We recorded 2D and 3D topographic AFM images of the photoresist templates possessing square contact hole arrays at a resolution of 1 μm. Fig. 5a displays the square hole textures of the photoresist. Fig. 5b and c presents 2D and 3D topographic AFM images of the arrays of the PS-*b*-PNIPAAm brush pillars at 0.2 and 2 V, respectively. At 0.2 V, the PS-*b*-PNIPAAm brush pillars had a uniform height of 325 nm and a width of 1 μm. After increasing the voltage to 2 V, however, the pillar height decreased by approximately 12 nm and the width increased by approximately 33 nm; that is, thermally responsive behavior was manifested as collapse of the PNIPAAm. In addition, we recorded roughness, determined from AFM height images in the area of 10 μm × 10 μm, of flat and pillar arrays of Si–PS and Si–PS-*b*-PNIPAAm surfaces at 0.2 and 2 V in Table 1. Thermally responsive morphology resulted after copolymer grafting because the PNIPAAm blocks feature terminal groups, thereby generating switching properties in terms of the roughness. Furthermore, we determined the SWCA by fitting a Young–Laplace curve around the drop. Heterogeneous (chemically or geometrically) surfaces typically exhibit contact angle hysteresis; the earliest modeling of liquid drops on rough surface was performed by Wenzel [30] and Cassie and Baxter [31]. If a liquid fills up the rough surface to form a completely wetted contact with the surface, the system is said to exist in the Wenzel state; if, however, a liquid droplet sits on a composite surface composed of solid and air, it is said to occupy the Cassie state. Fig. 6a presents the voltage-dependence of the tethered PS-*b*-PNIPAAm pillar array in terms of SWCAs. The SWCAs increased substantially with applying voltage from 0.2 to 2 V, implying that the LCST of the PNIPAAm was close to 33–38 °C, consistent with reports indicating that it is ca. 35 °C [37,38]. Below LCST, the PNIPAAm brushes underwent primarily intermolecular hydrogen bonding with water molecules, providing a hydrophilic PNIPAAm film. We also summarized SWCAs and hysteresis, calculated from the advancing and receding WCAs of droplets, of flat and pillar arrays of Si–PS and Si–PS-*b*-PNIPAAm surfaces at 0.2 and 2 V in Table 1. Both of the Si–PS on flat and nanopillar surfaces remained similar SWCAs at 0.2 and 2 V. Apparently, the pillar structure of PS brush enhanced the hydrophobic property on the surface, consistent with other reports [39]. After block copolymerization with PNIPAAm, the PS-*b*-PNIPAAm copolymer brush exhibited higher SWCAs at 2 than at 0.2 V because of the addition of PNIPAAm segments, corresponding other reports [40]. We defined the difference of the SWCAs below and above LCST as a thermally responsive efficiency of SWCA ($\Delta\theta_{eff} = SWCA_{50°C} - SWCA_{25°C}$) during the phase transition. The pillar array of the PS-*b*-PNIPAAm possessed the higher thermally responsive efficiency of SWCA than that of flat surface due to the capillary/meniscus forces [41]. Furthermore, the SWCA of the pillar array of tethered PS-*b*-PNIPAAm brushes increased from 22.4 ± 4° to 117 ± 4° upon increasing the applying voltage from 0.2 to 2 V; it returned to 24.5 ± 4° after

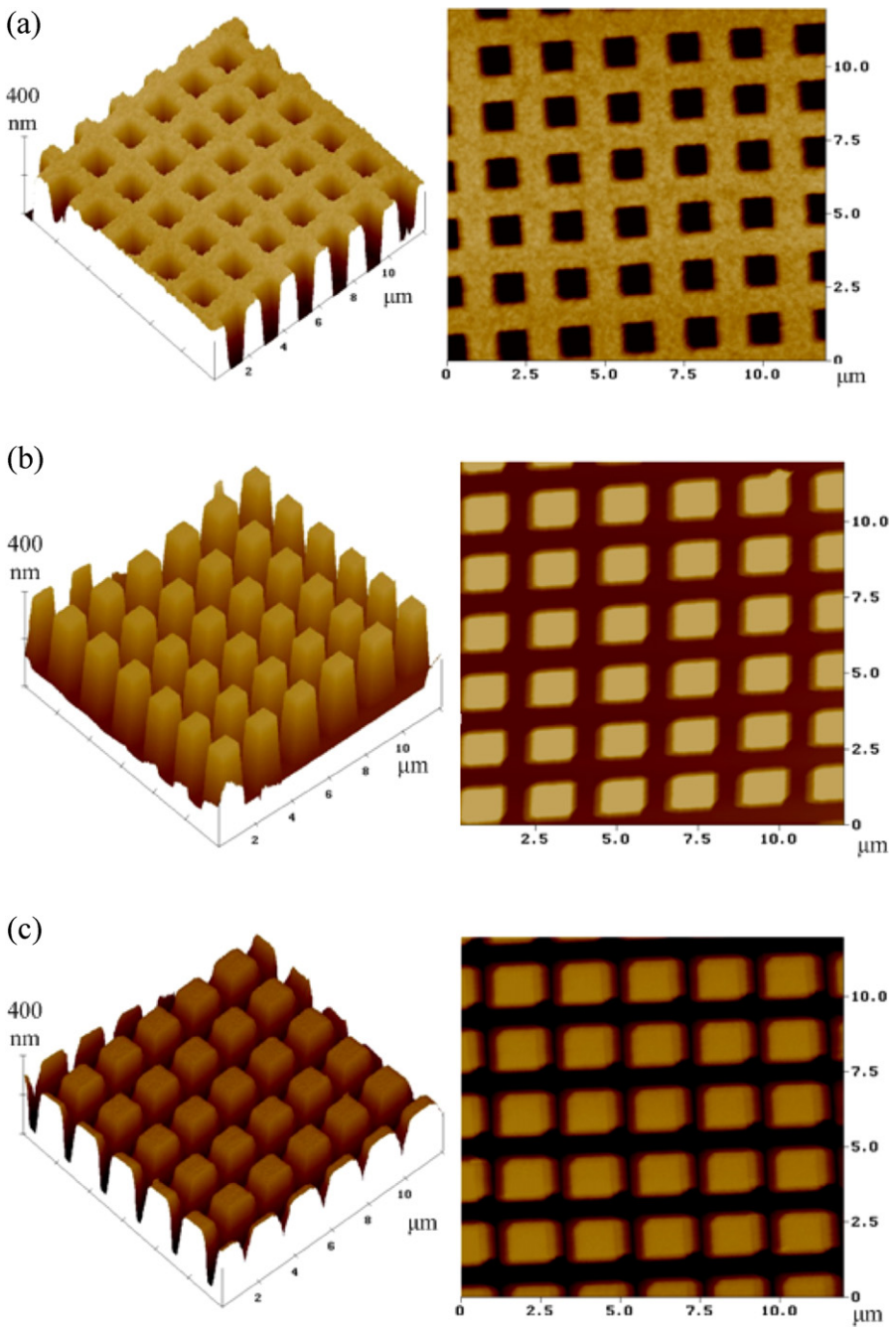

Fig. 5. 2D and 3D AFM height images (10 μm × 10 μm) of 1-μm resolution (a) contact hole arrays generated by e-beam lithography and pillar arrays of tethered PS-*b*-PNIPAAm brushes at (b) 0.2 and (c) 2 V.

Table 1
SWCAs hysteresis and roughness of flat and pillar arrays of Si–PS and Si–PS-*b*-PNIPAAm surfaces at 0.2 and 2 V.

Samples	SWCA (degree)		Hysteresis[a]		Roughness[b] (nm)	
	0.2 V	2 V	0.2 V	2 V	0.2 V	2 V
Flat Si–PS layer	63.9	65.7	10.1	9.2	3.4	3.8
Flat Si–PS-*b*-PNIPAAm layer	37.5	81.5	7.1	5.4	6.6	2.9
Si–PS pillar surface	95.7	95	14.3	13.5	155.2	144.1
Si–PS-*b*-PNIPAAm pillar surface	21.7	102.5	41	5.9	158.4	122.6

[a] Calculated from the advancing and receding WCAs of droplets.
[b] Determined from AFM height images in the area of 10 μm × 10 μm.

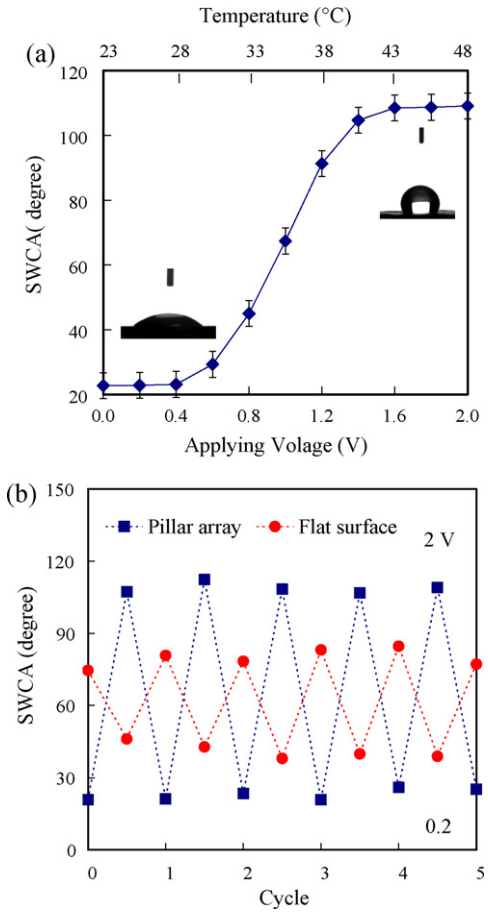

Fig. 6. (a) SWCAs of tethered PS-*b*-PNIPAAm copolymer surface plotted as a function of the applying voltages through the multi-layer thin film. (b) SWCAs of the pillar array and flat surfaces of the tethered PS-*b*-PNIPAAm brushes after four cycles of varying the voltages between 0.2 and 2 V.

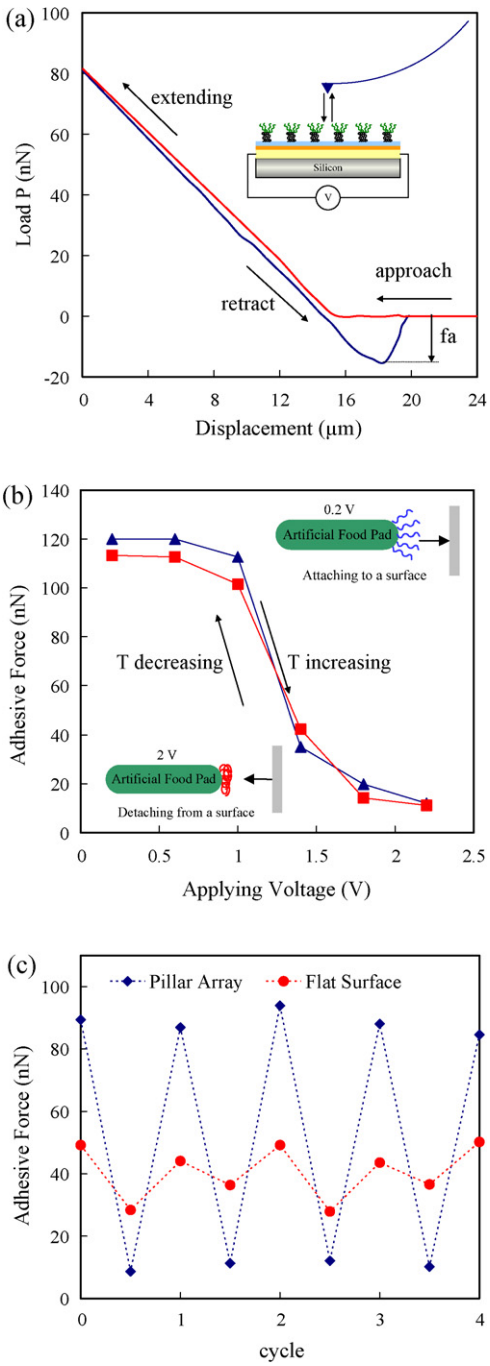

Fig. 7. (a) Load–displacement curve obtained from the pillar array. A sawtooth profile can be observed during retraction before pull-off occurs. (b) Changes in adhesive forces of the tethered PS-*b*-PNIPAAm pillar plotted as a function of applying voltages. Insets: Illustrations of the artificial foot pad alternately attaching to and detaching from a surface through transitions of the terminus from brush to globule structures upon switching the voltage between 0.2 and 2 V. (c) Adhesive forces of pillar array and flat surface of the tethered PS-*b*-PNIPAAm brushes after four cycles voltage tuning between 0.2 and 2 V.

decreasing temperature from 2 to 0.2 V. For the copolymer brush, this behavior was reversible for five cycles (Fig. 6b).

We recorded the dynamic WCAs (advancing and receding contact angles) on the pillar structure surfaces to determine their hysteresis at 0.2 and 2 V, respectively. The contact angle hysteresis ($\Delta\theta$) can be used to determine the state of a liquid droplet. If the contact angle hysteresis is small (large), then the droplet exists in the Cassie (Wenzel) state. Thus, the contact angle hysteresis is responsible for the pinning of liquid droplets on a surface. A discontinuity in the hysteresis exists when a transition occurs between the Wenzel and Cassie states. In our case, a liquid droplet sat on a composite surface composed of solid and air. At 0.2 V, the PS-*b*-PNIPAAm pillar array existed in the Wenzel state because of higher hysteresis (Table 1); the system resided in the Cassie state at 2 V because of lower hysteresis. Thus, a transition occurred between the Wenzel and Cassie states during voltage tuning. In the absence of the pillar structure, the hysteresis remained almost constant at 0.2 and 2 V. Thermally responsive properties resulted after copolymer grafting because the PNIPAAm blocks feature terminal groups that are thermally responsive, thereby generating switching properties in terms of the contact mode (Wenzel or Cassie state).

Adhesion is generally determined in terms of the amount of force necessary to separate two surfaces in contact. The geometry of the adhesion tests with a representative experimental force–distance curve obtained on patterned surfaces with pillars of Si–PS-*b*-PNIPAAm along 80 μm of scanning distance is depicted in Fig. 7a. During loading, the curves initially show a nonlinear response related to the change in the stiffness as the number of pillars in contact increased. No significant approach-retraction hysteresis could be noticed, indicating that the deformation of the sample is predominantly elastic, and viscoelastic effects, while present, can be neglected. During retraction, the curves showed several points of instability where the force changed abruptly. The resulting sawtooth profile was associated with isolated detachment events of the peripheral pillars in the contact area. These effects were not seen when measuring adhesion to a planar surface.

The final detachment event gives the value of the adhesive force (P_{ad}). The influence of the fabrication procedure, the environmental conditions (temperature and humidity), and the experimental parameters (indentation rate and preload) on the adhesion results were first tested and later carefully controlled to allow meaningful comparison of data obtained from different specimens. The time elapsed between the fabrication process and the adhesion measurements was critical for reproducibility. Changes in humidity can also influence the experimental P_{ad} values, as liquid bridges around the contact areas result in higher adhesion. Meniscus forces on patterned surfaces depend on the geometry and radius of the contact surfaces, the hydrophobicity of the materials [41]. Adhesion is generally obtained by the amount of force necessary to separate two surfaces in contact and the results (Fig. 7a). We observed that the adhesive forces were closely related to the micropillar structure of the PS-*b*-PNIPAAm brushes, but they were also influenced strongly by the thermally responsive properties of the PNIPAAm blocks, as revealed in Fig. 7b. The adhesive force on the PS-*b*-PNIPAAm pillars decreased abruptly upon increasing the voltage from 0.2 to 2 V. The two insets to Fig. 7b illustrate an artificial food pad alternately attaching to and detaching from a surface through terminal transitions from brushes to globules upon increase the applying voltage from 0.2 to 2 V. We determined the thermally responsive efficiencies of the adhesive force (P_{eff}) of the copolymer-modified thin film surfaces from calculations of the adhesive force at 0.2 and 2 V. Compared with the flat PS-*b*-PNIPAAm surface, the copolymer surface featuring the pillar arrays exhibited a significantly enhanced value of P_{eff}. This thermal switching of the adhesive force of the copolymer brush pillars was reversible for at least four cycles (Fig. 7c), whereas that of the flat surface of PS-*b*-PNIPAAm copolymer brushes was barely evident.

The results suggest that the thermally switchable efficiency of adhesive force of PS-*b*-PNIPAAm pillar could be enhanced by the structure of pillar array. The advantage of the thermally switchable adhesion described here is the potential to biomimetic foot pad of lizards with the ability of alternately attaching and detaching from a surface where they climb. It is well established that adhesive force is determined by two important factors: contact interfacial forces and noncontact forces such as van der Waals, electrostatic forces, and capillary/meniscus forces [42]. At first, the adhesive force is closely related to the real contact area between the tip and surface; a larger area leads to a larger adhesive force. With the structure of pillar array, the tip traveling between the pillars results in the decrease of the contact area, responsible for decreased adhesive force [43]. Second, when the solid surfaces were hydrophilic, they would easily form a meniscus by the adsorbed water molecules, thus they had larger adhesive forces. However, when the surfaces were hydrophobic, they would show lower adhesion [44]. The terminal PNIPAAm brush at 2 V increases the surface hydrophobicity of pillar copolymer surfaces, which leads to the reduction of adhesive force. Therefore, surface textures and contact area of thermally responsive property were combined that can be used to generate biomimetic analogues.

To investigate the biological attachment and detachment property, we measured the friction force on the copolymer pillar surface of PS-*b*-PNIPAAm pillar under a normal load of 200 nN by AFM/FFM at 0.2 and 2 V, respectively. The friction force is given here in the form of voltage signal, which is proportional to the real friction force [45]. Therefore, the results from various surfaces could be compared to each other. Reproducibility for friction forces is ±3% for all measurements under a normal load of 200 nN. As seen from Fig. 8a, friction force data also follows a similar trend to the adhesion data for the aspect ratios at 0.2 and 2 V. The friction force of the PS-*b*-PNIPAAm pillar decreases rapidly at ca. 1.2 V due to the hydrophobic property of PNIPAAm. The two insets to Fig. 8a illustrate Wenzel and Cassie states of an artificial food pad

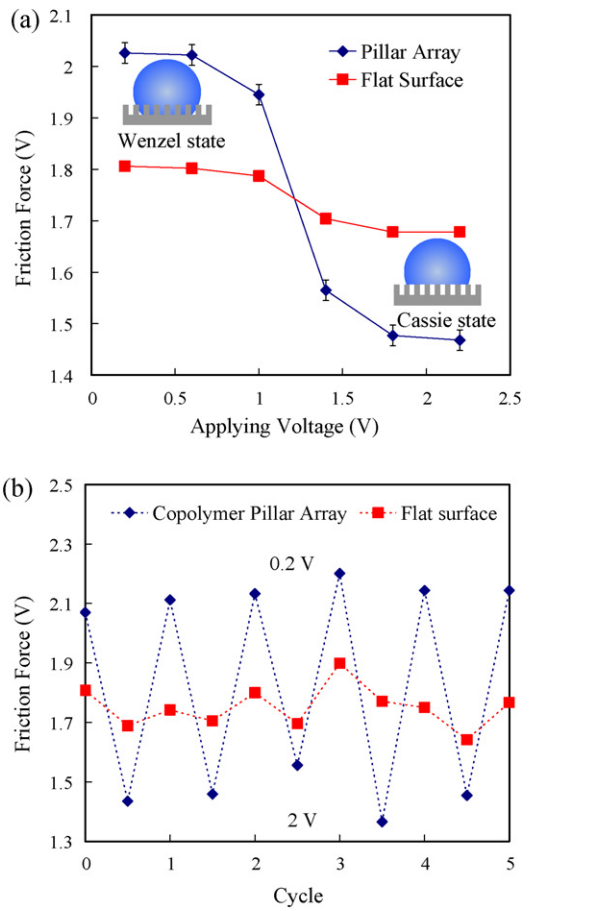

Fig. 8. (a) Changes in friction forces under a normal load of 200 nN on the PS-*b*-PNIPAAm pillar array surfaces at 0.2 and 2 V. (b) Friction forces on the copolymer pillar array and flat surface of the tethered PS-*b*-PNIPAAm after five cycles voltage tuning between 0.2 and 2 V. Insets: Illustrations of the artificial foot pad alternately attaching to and detaching from a surface through transitions of Wenzel and Cassie state upon switching the voltage between 0.2 and 2 V.

during terminal transitions from brushes to globules upon increase the applying voltage from 0.2 to 2 V. Compared with the flat PS-*b*-PNIPAAm surface, the tethered copolymer with pillar textures obviously generated the thermally switchable friction forces. The real area of contact and surface chemistry affect friction force at nanoscale in dry/wet contacts strongly [45]. The real area of contact is dependent upon the area density and height of pillars. With the same tip scan velocity through the pillars, the number of asperities in contact is reduced greatly which lead to the real area of contact reduced and so lead to low friction force. Then, if the surface is hydrophilic, it is easy to form capillary meniscus by them or the adsorbed water molecules, which would lead to large shearing strength and higher friction [44]. In other words, if the surface is hydrophobic, it would get the opposite result. The contact regime of PNIPAAm made the surface more hydrophilic and hydrophobic which lead to higher and lower surface energy at 0.2 and 2 V, respectively. This thermally switchable behavior of the tethered copolymer pillar on friction force was reversible for five cycles (Fig. 8b). Without texture structure of the tethered copolymer brushes, the reversibly thermally responsive behavior on friction force was irregular. The mechanism responsible for the obtained inaccuracy may be “stick–slip” phenomenon, in which, during the stick phase, the friction force builds up to a certain value and, once a large enough force has been applied to overcome the static friction force, slip occurs at the interface.

4. Conclusions

We have fabricated a biomimetic device with PS-*b*-PNIPAAm copolymer pillars to develop alternate attaching to and detaching from surfaces through variations in thermally switchable adhesion or friction force upon switching the temperature below and above LCST of PNIPAAm through applying voltage. The well-defined PS-*b*-PNIPAAm copolymer pillar array on the biomimetic device substantially matches with the biological system of climbing aptitude, alternate attaching to and detaching from a surface through thermally switchable adhesion or friction force. The results show that thermally switchable performance of the copolymer pillars on adhesion could be apparently enhanced by the copolymer pillars. It is expected that this paper could provide additional insight on the biomimetic foot pad by tailoring the surface topography and using stimuli-responsive hydrogels as the contact regime. We intend to employ this processing strategy to create biomimetic versions of lizards' foot pads, with the ability to alternately attach and detach from, and thereby climb up, a surface.

Acknowledgment

We thank the National Science Council of the Republic of China for supporting this research financially.

References

[1] J.-K. Chen, J.-H. Wang, S.-K. Fan, J.-Y. Chang, Journal of Physical Chemistry C 116 (2012) 6980–6992.
[2] A. del Campo, C. Greiner, I. Alvarez, E. Arzt, Advanced Materials 19 (2007) 1973–1977.
[3] Z.D. Dai, J.R. Sun, Progress in Natural Science 17 (2007) 1–5.
[4] Y. Tian, N. Pesika, H.B. Zeng, K. Rosenberg, B.X. Zhao, P. McGuiggan, K. Autumn, J. Israelachvili, Proceedings of the National Academy of Sciences of the United States of America 103 (2006) 19320–19325.
[5] H. Lee, B.P. Lee, P.B. Messersmith, Nature 448 (2007) 338–342.
[6] K. Autumn, Y.A. Liang, S.T. Hsieh, W. Zesch, W.P. Chan, T.W. Kenny, R. Fearing, R.J. Full, Nature 405 (2000) 681–685.
[7] G. Huber, S.N. Gorb, R. Spolenak, E. Arzt, Biological Letters 1 (2005) 2–4.
[8] W. Sun, P. Neuzil, T.S. Kustandi, S. Oh, V.D. Samper, Biophysical Journal 89 (2005) L14–L16.
[9] C. Greiner, A. del Campo, E. Arzt, Langmuir 23 (2007) 3495–3502.
[10] W.K. Cho, I.S. Choi, Advanced Functional Materials 18 (2008) 1089–1096.
[11] M.T. Northen, K.L. Turner, Nanotechnology 16 (2005) 1159–1166.
[12] A.J. Crosby, M. Hageman, A. Duncan, Langmuir 21 (2005) 11738–11743.
[13] A.K. Geim1, S.V. Dubonos, I.V. Grigorieva, K.S. Novoselov1, A.A. Zhukov, Yu.S. Shapoval, Nature Materials 2 (2003) 461–463.
[14] M.T. Northen, K.L. Turner, Sensors and Actuators A 130-131 (2006) 583–587.
[15] B. Yurdumakan, N.R. Raravikar, P.M. Ajayan, A. Dhinojwala, Chemical Communications 30 (2005) 3799–3801.
[16] J.-K. Chen, B.-J. Bai, F.-C. Chang, Applied Physics Letters 99 (2011) 013701.
[17] J.K. Chen, C.H. Chan, F.C. Chang, Applied Physics Letters 92 (2008) 053108.
[18] T.-Y. Chen, J.-K. Chen, Colloid and Polymer Science 289 (2011) 433–445.
[19] J.-K. Chen, B.-J. Bai, F.-C. Chang, Journal of Physical Chemistry C 115 (2011) 21341–21350.
[20] N.A. Peppas, J.Z. Hilt, A. Khademhosseini, R. Langer, Advanced Materials 18 (2006) 1345–1360.
[21] C.H. Chan, J.K. Chen, F.C. Chang, Sensors and Actuators B 13 (2008) 327–332.
[22] J.-K. Chen, P.-C. Pai, J.-Y. Chang, S.-K. Fan, ACS Applied Materials Interfaces 4 (2012) 1935–1947.
[23] J.-K. Chen, J.-Y. Li, Sensors and Actuators B 150 (2010) 314–320.
[24] J.-K. Chen, J.-Y. Li, Journal of Colloid and Interface Science 358 (2011) 454–461.
[25] J.K. Chen, A.L. Zhuang, Colloid and Polymer Science 289 (2011) 1283–1294.
[26] J.K. Chen, C.Y. Hsieh, C.F. Huang, P.M. Li, S.W. Kuo, F.C. Chang, Macromolecules 41 (2008) 8729–8736.
[27] J.-K. Chen, C.-Y. Hsieh, C.-F. Huang, P.-M.J. Li, Journal of Colloid and Interface Science 338 (2009) 428–434.
[28] W. Zhao, L. Wang, Q. Xue, ACS Applied Materials Interfaces 2 (2010) 788–794.
[29] L.C. Gao, T.J. McCarthy, Langmuir 22 (2006) 6234.
[30] R.N. Wenzel, Industrial and Engineering Chemistry 28 (1936) 988–994.
[31] A.B.D. Cassie, S. Baxter, Transactions Faraday Society 40 (1944) 546–551.
[32] J.K. Chen, T.-Y.J. Chen, Journal of Colloid and Interface Science 355 (2011) 359–367.
[33] J.-K. Chen, Z.-Y. Chen, H.-C. Lin, P.-D. Hong, F.-C. Chang, ACS Applied Materials Interfaces 1 (2009) 1525–1532.
[34] J.K. Chen, A.-L. Zhuang, Journal of Physical Chemistry C 114 (2010) 11801–11809.
[35] Q. Yu, Y. Zhang, H. Chen, F. Zhou, Z. Wu, H. Huang, J.L. Brash, Langmuir 26 (2010) 8582–8588.
[36] S.R. Wasserman, Y.-T. Tao, G.M. Whitesides, Langmuir 5 (1989) 1074–1087.
[37] J.-K. Chen, J.-Y. Li, Applied Physics Letters 97 (2010) 063701.
[38] Z. Zhu, C.C. Wu, H.P. Liu, Y. Zou, X.L. Zhang, H.Z. Kang, C.J. Yang, W.H. Tan, Angewandte Chemie International Edition 49 (2010) 1052–1056.
[39] K.-Y. Yeh, L.-J. Chen, Langmuir 24 (2008) 245–251.
[40] L. Li, Y. Zhu, B. Li, C. Gao, Langmuir 24 (2008) 13632–13639.
[41] Y.F. Mo, W.J. Zhao, D.M. Huang, F. Zhao, M.W. Bai, Ultramicroscopy 109 (2009) 247–252.
[42] Z. Burton, B. Bhushan, Nano Letters 5 (2005) 1607–1613.
[43] Y.I. Rabinovich, J.J. Adler, A. Ata, R.K. Singh, B.M. Moudgil, Journal of Colloid and Interface Science 232 (2000) 17–24.
[44] W.J. Zhao, M. Zhu, Y.F. Mo, M.W. Bai, Colloids and Surfaces A 332 (2009) 78–82.
[45] S.Y. Song, S.L. Ren, J.Q. Wang, S.R. Yang, J.Y. Zhang, Langmuir 22 (2006) 6010–6015.

Biographies

Jem-Kun Chen received his BS degree (1996) and MS (1998) in chemical engineering from National Tsing Hua University, and PhD degree (2003) in applied chemistry from National Chiao Tung University, Taiwan. From 2003 to 2005, he was a postdoctoral fellow with Prof. Samukawa at the Department of Fluid Science at Touhoku University, Sendai in Japan, where he worked on the research about the fabrication and analysis of quantum dot and nanodisk. He returned to the department of polymer engineering in National Taiwan University of Science and Technology, as an assistant professor from 2006 to 2010. He is currently an associate professor of materials science and technology in National Taiwan University of Science and Technology from 2006 to now. Dr. Chen's current research emphasizes fabrication process, characterization, modeling, and optimization of polymer brush devices for optical and biological sensors. He has published over 30 articles (2007–2012).

Jing-Hong Wang received his MS degree (2010) in our lab from the Department of Materials Science and Engineering, National Taiwan University of Science and Technology. His research interests are centered mainly in the development of advanced polymer brush technology. He works currently for AUO Company as a process engineer.

Chih-Chia Cheng received his PhD degree (2008) from the Department of Applied Chemistry, National Chiao-Tung University, Taiwan. From 2008 to now, he is a postdoctoral in Department of Applied Chemistry, National Chiao-Tung University, where he worked on the research about the synthesis of the self-assembled macromolecule. He has published over 10 articles (2008–2012).

Fu-Hsiang Ko received his PhD degree (1996) from the Department of Nuclear Science, National Tsing Hua University, Taiwan. From 1992 to 1996, he was a Researcher at National Nano Device Laboratories (NDL), where he worked on the research about the nanofabrication including top-down approach and bottom-up approach. In 2005, he returned to the Institute of Nanotechnology in National Chiao-Tung University, as a Professor to now. Dr. Ko's current research emphasizes nanodevices of biosensors and electronic devices. He has published over 40 articles (2004–2012).